



Cite this: *New J. Chem.*, 2017, 41, 358

# Fluorescent benzimidazo[1,2-a]quinolines: synthesis, spectroscopic and computational studies of protonation equilibria and metal ion sensitivity†

Marijana Hranjec,<sup>a</sup> Ema Horak,<sup>b</sup> Darko Babić,<sup>c</sup> Sanela Plavljanin,<sup>a</sup> Zrinka Srdović,<sup>a</sup> Ivana Murković Steinberg,<sup>b</sup> Robert Vianello\*<sup>d</sup> and Nataša Perin\*<sup>a</sup>

We describe the UV-Vis and fluorescence spectroscopic characterization of newly synthesised amino and diamino substituted benzimidazo[1,2-a]quinolines and their various 1:1 metal complexes together with the related computational analysis of their acid/base properties and metal binding affinities. The work was performed in order to evaluate the photophysical features of these compounds and assess their potential chemosensor activity towards pH and metal ions in several polar and non-polar organic solvents. In addition, pH titrations and titration with metal chloride salts were carried out to determine the selectivity towards  $\text{Co}^{2+}$ ,  $\text{Cu}^{2+}$ ,  $\text{Ni}^{2+}$  and  $\text{Zn}^{2+}$  cations and explore their potential as chemosensors and pH probes. While all systems exhibit notable but impractical differences in sensitivities and spectral responses with the used metals, computational analysis aided in identifying benzimidazo[1,2-a]quinolines mono- and disubstituted with the piperazine fragment as very promising and efficient pH sensors in the acidic environment, particularly in the range of  $\text{pH} \approx 3$ , which is extended to  $\text{pH} \approx 6$  upon the addition of metal cations. Their analytical features are significantly better than those involving the chain amino substituents, and their further development is strongly suggested.

Received (in Montpellier, France)  
20th July 2016,  
Accepted 9th November 2016

DOI: 10.1039/c6nj02268e

www.rsc.org/njc

## Introduction

Optical sensors are widely used in biochemical and medicinal studies for the detection of biologically important molecules, and various cations and anions. Fluorescence spectroscopy in particular has long been viewed as a powerful tool for basic research in the biological sciences due to the notable progress made in instrumentation, and the synthesis and availability of novel fluorophores.<sup>1–4</sup> The selective recognition and detection of transition metal cations are of great interest for many scientific studies due to their importance in chemical, biological, biomedical or environmental processes.<sup>5–7</sup> Many of them are involved in the most important biological and biochemical processes, such as transmission of nerve impulses, muscle

contraction and regulation of cell activity.<sup>8</sup> For example,  $\text{Zn}^{2+}$  is an essential trace metal element responsible for the control of many cellular and enzymatic processes in living organisms, and it is also a contributory factor in neurological disorders, such as epilepsy and Alzheimer's disease.<sup>9,10</sup> Also,  $\text{Zn}^{2+}$  has a specific structural function that allows the formation of peptides into multiple domains, or “zinc fingers”, by the coordination to amino acids like cysteine and histidine. Importantly, high levels of Zn can be cytotoxic and may cause serious problems such as skin disease, diabetes and some types of carcinoma.  $\text{Co}^{2+}$  is mainly retrieved in the corrin ring of vitamin B12, which is the original Co storage in biological systems, and is essential for the growth and metabolism of plants.  $\text{Cu}^{2+}$  is another necessary and important trace element, the third most abundant transition metal in the body and in the brain, responsible for the normal function of many tissues, like the immune system, the nervous system and the heart.<sup>11</sup>  $\text{Ni}^{2+}$  is a nutritionally essential trace metal in several animal species, microorganisms and plants. On the other hand, fluorescent pH probes are widely used in analytical and biomedical chemistry,<sup>12</sup> for measuring inter-cellular  $\text{pH}^{13,14}$  or monitoring pH in blood.<sup>15</sup> Such probes are vital for the development of chemical sensors for biomedical diagnostics, cell biology and environmental monitoring.<sup>16,17</sup> In summary, fluorescent sensors that provide high sensitivity, good selectivity, and rapid response are widely available and

<sup>a</sup> Department of Organic Chemistry, Faculty of Chemical Engineering and Technology, University of Zagreb, Marulićev trg 20, HR-10000 Zagreb, Croatia. E-mail: nperin@fkit.hr

<sup>b</sup> Department of General and Inorganic Chemistry, Faculty of Chemical Engineering and Technology, University of Zagreb, Marulićev trg 19, HR-10000 Zagreb, Croatia

<sup>c</sup> Group for Computational Life Sciences, Ruđer Bošković Institute, Bijenička 54, HR-10000 Zagreb, Croatia

<sup>d</sup> Computational Organic Chemistry and Biochemistry Group, Ruđer Bošković Institute, Bijenička 54, HR-10000 Zagreb, Croatia. E-mail: robert.vianello@irb.hr

† Electronic supplementary information (ESI) available: Job's plots, spectroscopic data for precursors 1–2, calculated spectra and difference densities, correlation between computed and measured first excitation. See DOI: 10.1039/c6nj02268e



support multiple modes of detection.<sup>18</sup> Their structure requires at least two functional sites: a recognition site where the host binds to the analyte, and a fluorophore which provides a spectroscopic signal dependent on the interaction with the analyte. Such response is mostly guided by the well-known photo-physical mechanisms of electron or charge transfer.<sup>19</sup> The main challenge in the design and synthesis of novel fluorescent compounds for sensing applications is in providing both essential functions, recognition and signal transduction, in one molecule.

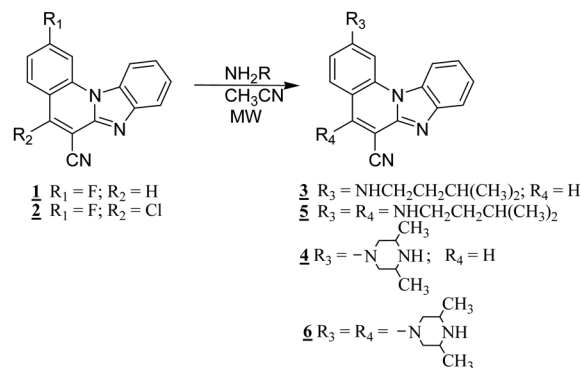
One of the most extensively studied classes of organic fluorescent sensors is that based on heterocyclic compounds,<sup>20,21</sup> which have excellent spectroscopic properties and selectively bind to essential cations and anions. Thus, they can be employed as sensitive and selective optical sensors in a wide range of biological, environmental, and chemical processes. Besides the fact that they are widely incorporated in the structure of numerous important natural and synthetic biochemical agents, benzimidazole and especially their benzannulated derivatives, due to the possession of a highly conjugated planar chromophore, offer promising applications in optoelectronics, optical lasers, fluorescence probes, organic luminophores or fluorescent dyes in traditional textile and polymer fields.<sup>22,23</sup> A great variety of heterocyclic molecules have been employed for the development of optical sensors where the benzimidazole unit is one of the most important key building blocks.<sup>24–28</sup> Additionally, the fluorescence of cyclic benzimidazole derivatives can be significantly altered by additional substituents placed on different positions of the planar chromophore or by condensation with other heterocycles, which leads to the extension of the conjugated aromatic surface.<sup>29</sup> Recently, we explored the characteristics of 2-amino-5-phenylbenzimidazo[1,2-*a*]quinoline-6-carbonitrile as a selective chemosensor for detecting versatile metal cations. Importantly, the fluorescence intensity of this compound significantly increases upon the addition of Zn<sup>2+</sup>.<sup>30</sup>

Encouraged by the confirmed optical properties and application possibility of a biologically active amino substituted benzimidazo[1,2-*a*]quinoline skeleton for the detection of various cations in solution, we set out the spectroscopic and computational characterization of several 2-amino and 2,5-diamino substituted benzimidazo[1,2-*a*]quinolines by means of UV-Vis and fluorescence spectroscopy, density functional theory calculations, pH titrations and UV-Vis and fluorescence titrations with several metal cations in various polar and non-polar organic solvents.

## Results and discussion

### Synthesis

All newly prepared compounds were synthesized according to the previously published synthetic procedures. The main procedure is shown in Scheme 1. Based on the series of undertaken experiments in order to optimize the reaction times and yields, targeted amino and diamino substituted benzimidazo[1,2-*a*]quinolines 3–6 were finally prepared from the corresponding halogeno or dihalogeno substituted precursors 1–2 using uncatalyzed microwave assisted amination in low to moderate yields (28% to 33%).



Scheme 1 Synthesis of compounds 3–6.

This reaction was performed in acetonitrile with an excess of five equivalents of the corresponding amine at 800 W power, 170 °C and 40 bar, while targeted compounds were purified by using column chromatography on silica gel.

The structures of all prepared systems were determined by NMR analysis based on inspecting H–H coupling constants, chemical shifts and by mass spectroscopy. Generally, <sup>1</sup>H NMR spectra of all amino substituted benzimidazo[1,2-*a*]quinolines showed a downfield shift of the aromatic protons in comparison to halogeno substituted precursors 1–2. Also, the appearance of protons related to amino substituents in the aliphatic region can be observed in both <sup>1</sup>H and <sup>13</sup>C NMR.

### Spectroscopic characterization

In order to study spectroscopic properties of 3–6, UV-Vis and fluorescence emission spectra were recorded in several organic solvents selected to ensure good solubility. To study the influence of the chosen solvents on the spectroscopic characteristics of the tested compounds, stock solutions were prepared in two polar solvents, namely ethanol and acetonitrile and two non-polar solvents toluene and dioxane.

**UV-Vis absorption spectra.** UV-Vis spectra were measured in the range of 200–500 nm at the same concentration of  $2 \times 10^{-5}$  mol dm<sup>−3</sup> at room temperature (Fig. 1). The UV-Vis absorption spectra of 3 and 4 showed two main bands at 380–440 nm while diamino substituted 5 and 6 displayed three main bands at 360–420 nm, which we assign to  $\pi$ – $\pi^*$  and  $n$ – $\pi^*$  electronic transitions involving amino substituents. Absorption bands in the region from 250 to 325 nm are assigned to the moderate energy transition of the tetracyclic conjugated aromatic  $\pi$ -system. Considering the UV-Vis spectra of 3, measured in four mentioned solvents, the most intensive absorbance with a strong hyperchromic effect and a slight bathochromic shift was observed in ethanol, while in acetonitrile a significant hypochromic effect was noticed. Non-polar solvents, toluene and dioxane, also caused a significant hypochromic effect of the absorbance intensity as well as a slight hypsochromic shift of the absorbance maxima at 8 nm. The recorded spectra of 4 suggest that in non-polar solvents and acetonitrile this system shows the hyperchromic effect of the absorbance intensity relative to ethanol, and the hypsochromic shift of the absorbance maxima at 5 ppm. The similar behaviour



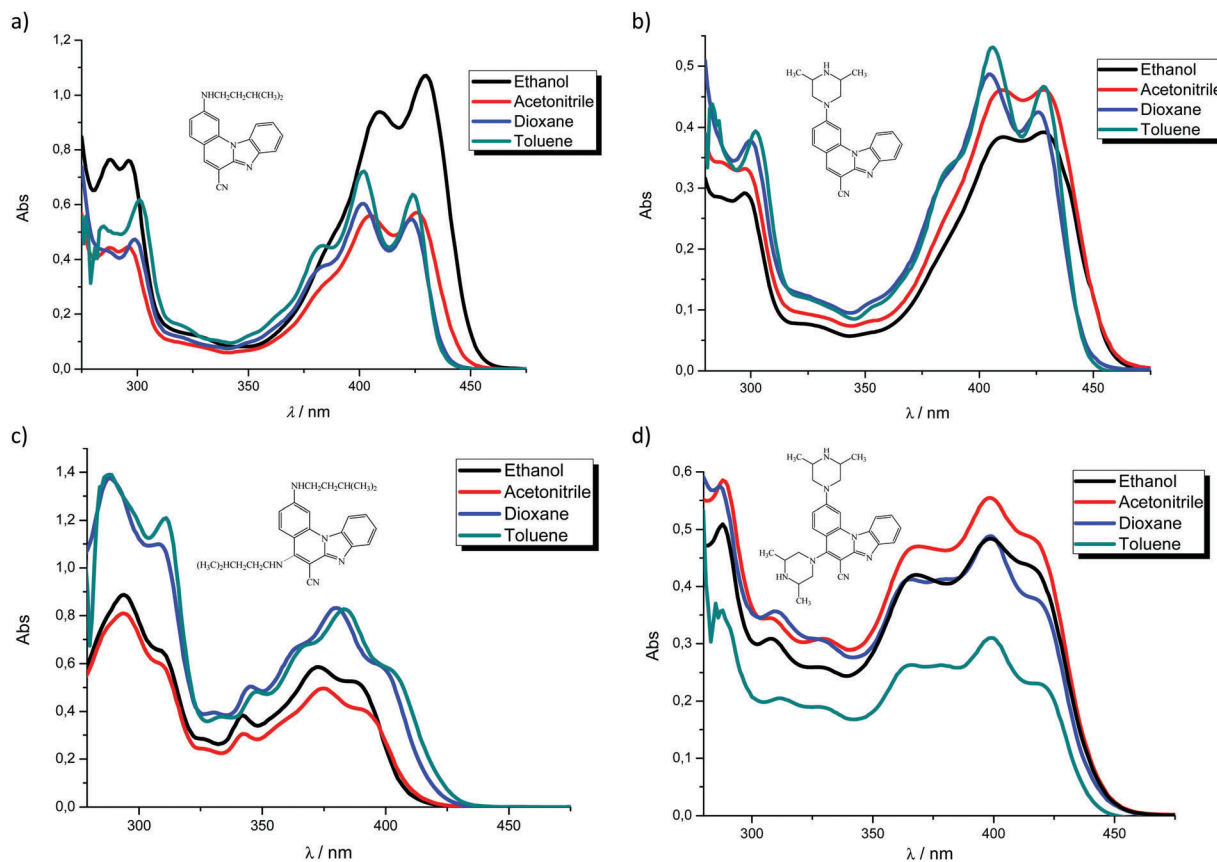


Fig. 1 UV-Vis spectra recorded in ethanol, acetonitrile, dioxane and toluene at concentrations of  $2 \times 10^{-5} \text{ mol dm}^{-3}$  of **3** (a), **4** (b), **5** (c) and **6** (d).

was observed for **5** since both non-polar solvents caused a hyperchromic effect of absorbance intensity and a bathochromic shift of absorbance maxima for around 8–10 nm. Furthermore, **6** showed the highest absorbance intensity in acetonitrile while in toluene the intensity drastically decreased.

**Fluorescence emission spectra.** Fluorescence emission spectra of **3–6** were recorded at the same concentration of  $1 \times 10^{-7} \text{ mol dm}^{-3}$  at room temperature (Fig. 2). Emission spectra of **3** in polar solvents showed one main emission band with a slight bathochromic shift of maxima in ethanol while in toluene and dioxane it showed two main bands with maxima at 434 and 461 nm, respectively, with a small bathochromic shift in dioxane at 437 and 464 nm. In addition, **3** showed a significant increase of the emission intensity in non-polar solvents. **4** also revealed very similar behaviour with a significant decrease of the emission intensity in acetonitrile. Furthermore, **5** showed one main band in all solvents with the highest emission intensity in ethanol and a bathochromic shift of maxima in dioxane and toluene for around 13 nm. **6** exhibited one main band in all solvents with the highest emission intensity in dioxane while in acetonitrile the latter drastically decreased. 2-*N*-Isopentylamino substituted **3** revealed the highest quantum yield while 2,5-diamino derivatives showed very low yields (0.04 for **5** and 0.01 for **6**). Electronic absorption and fluorescence data for **3–6** are summarized in Table 1, while analogous data for halogen substituted precursors **1–2** are presented in Table S1 and Fig. S2 and S3 for comparison (ESI<sup>†</sup>).

### Effects of pH on spectral properties

Novel optical pH sensors and probes are usually characterized by their aqueous solution  $\text{pK}_a$  values determined by spectrophotometry or spectrofluorometry.<sup>1–4</sup> Optical evaluation of the concentrations of the acidic (HA) and basic forms ( $\text{A}^-$ ) is based on the Henderson–Hasselbach eqn (1):<sup>31</sup>

$$\text{pH} = \text{pK}_a + \log \frac{[\text{A}^-]}{[\text{HA}]} \quad (1)$$

Effects of pH on the spectral properties of **3–6** were determined by spectroscopic pH titrations. Their fundamental acid–base features, such as absorption ( $\lambda_{\text{abs}}$ ) and fluorescence maximum ( $\lambda_{\text{emiss}}$ ), the extinction coefficient ( $\epsilon$ ) and Stokes shifts ( $\nu_{\text{A}} - \nu_{\text{F}}$ ) are presented in Table 2.

The potential use of **3–6** as pH sensing probes is based on the spectral changes caused by the protonation of the basic nitrogen atoms within the molecules. Protonation of **3** and **5** with 0.1 M HCl causes a hypsochromic (blue) shift (12 nm) of the absorption band in the visible spectrum. On the other hand, protonation of **4** and **6** results in a bathochromic (red) shift (5–9 nm) due to a greater resonance effect and enhanced molecule stability. Different behaviours of these two sets of systems are significant for their application and will be rationalized using computational analysis (see later).



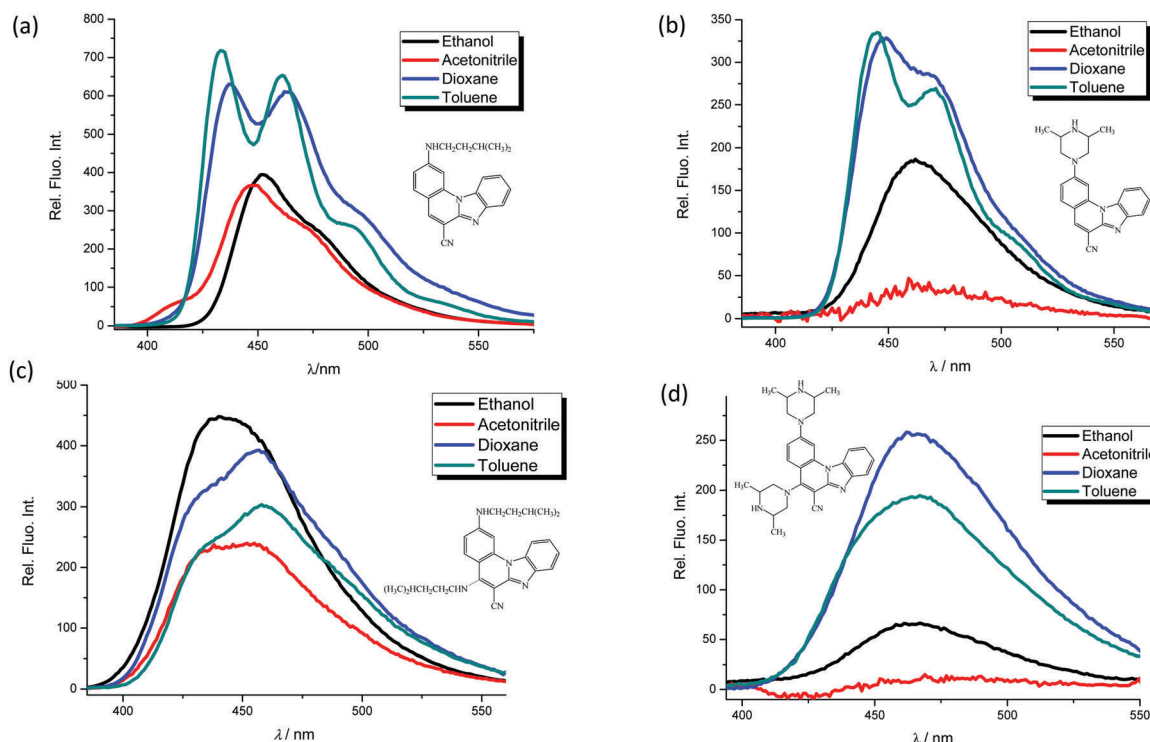


Fig. 2 Fluorescence emission spectra in ethanol, acetonitrile, dioxane and toluene at the concentration of  $1 \times 10^{-7} \text{ mol dm}^{-3}$  of **3** (a), **4** (b), **5** (c) and **6** (d),  $\lambda_{\text{exc.}} = 300 \text{ nm}$ .

Table 1 Electronic absorption and fluorescence emission data of studied compounds recorded at the same concentration in four organic solvents<sup>a,b</sup>

Compound Solvent	3				5				4				6			
	Eth	Acn	Dxn	Tol	Eth	Acn	Dxn	Tol	Eth	Acn	Dxn	Tol	Eth	Acn	Dxn	Tol
$\lambda_{\text{max}}$ (nm)	430	426	412	423	388	392	399	402	429	428	427	429	418	418	418	422
	409	403	399	401	372	374	380	382	409	410	404	405	399	397	399	400
	296	295	299	381	342	341	345	348	296	298	299	301	367	366	363	365
	287	270	274	300	294	294	308	311	272	272	267		330	331	328	
	271	250	252	283	262	263	297	287	250	250	252		307	309	310	
	248						264		232				288	289	280	
$\epsilon \times 10^3$ ( $\text{dm}^3 \text{ mol}^{-1} \text{ cm}^{-1}$ )	53.2	28.3	27.3	31.7	25.9	20.2	28.9	19.6	19.6	23.1	21.0	23.2	21.3	23.9	18.8	11.4
	46.6	27.6	30.4	36.1	29.2	24.9	41.8	41.0	19.2	23.0	24.4	26.6	24.3	27.6	24.3	15.5
	37.8	22.2	23.3	22.4	19.4	14.9	24.7	24.0	14.5	16.5	18.8	19.5	21.2	23.6	20.7	13.1
	37.8	33.5	38.4	30.3	44.2	40.2	54.6	60.3	11.7	14.3	16.9		12.8	15.4	15.6	
	50.9	27.6	31.9	25.9	34.7	37.0	68.9	69.2	9.8	12.0	15.1		15.5	17.1	16.7	
	44.2						84.6		8.8				25.4	29.2	28.9	
$\lambda_{\text{emiss}}$ (nm)	452	448	464	461	441	452	456	458	461	459	470	469	461	457	462	463
			437	433							449	444				
Rel. fluor. intensity	396	366	607	652	446	238	392	301	185	42	282	269	65	10	256	193
			624	719							328	333				
$\phi$	0.6760	—	—	—	0.1140	—	—	—	0.0482	—	—	—	0.0168	—	—	—

<sup>a</sup> Abbreviations Eth, Acn, Dxn and Tol correspond to ethanol, acetonitrile, dioxane and toluene, respectively. <sup>b</sup> The italicised wavelength values correspond to the most pronounced maximum in the visible region.

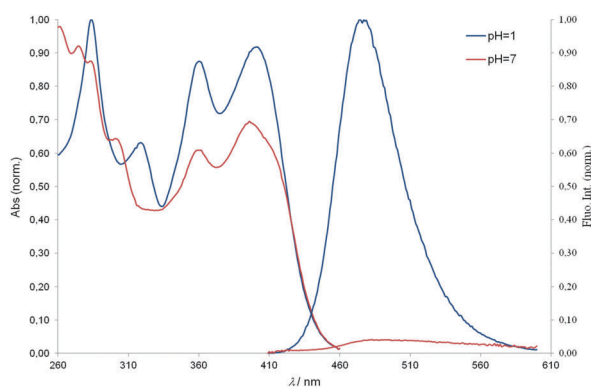
In general, the effect of pH is more pronounced in the fluorescence spectra than in the absorption spectra. The binding of a proton alters and expands  $\pi$ -conjugation and changes the electron-accepting nature of the aromatic moieties. Therefore, protonation can cause changes in both emission intensity and colour. It is known that the spectral properties of aminated benzimidazo[1,2-*a*]quinolines are related to charge transfer interactions.<sup>32</sup> As a result of protonation, the emission band

of all compounds is bathochromically shifted (20–45 nm) whilst the fluorescence intensity considerably increases for **3**, **4** and **6**, while it decreases for **5**. The spectral responses to pH for compound **6** are shown in Fig. 3. The Stokes shifts for **3** and **4** (Table 2) do not indicate large differences in energy upon excitation (6–45 nm), whilst the diamino substituted **5** and **6** had Stokes shift of up to 75 and 124 nm, which is significant for their potential application.



**Table 2** Effect of pH on the absorption and fluorescence emission properties of the studied compounds in universal buffer solutions

Compound	$\lambda_{\text{abs}}$ (nm)		$\epsilon \times 10^3$ (dm <sup>3</sup> mol <sup>-1</sup> cm <sup>-1</sup> )		$\lambda_{\text{emiss}}$ (nm)		Stokes shift (cm <sup>-1</sup> )		pK <sub>a</sub> <sup>c</sup>
	Acidic <sup>a</sup>	Neutral <sup>b</sup>	Acidic	Neutral	Acidic	Neutral	Acidic	Neutral	
<b>3</b>	293	422	25.61	13.70	476	456	1822	292	2.91
	438	450	26.84	14.03					
<b>5</b>	238	294	21.38	21.32	461	460	4693	3513	3.31
	305	344	18.20	11.22	503				
	343	375	10.32	14.77					
	379	392	9.42	14.57					
<b>4</b>	290	267	31.00	24.10	470	453	2143	2863	2.70 7.89
	425	284	31.03	16.90					
		397	16.20	19.45					
		416(sh)							
<b>6</b>	238	298	30.70	17.50	475	461	3885	3496	3.45 9.14
	283	358	28.10	16.60					
	317	394	17.70	18.70					
	359		24.60						
	399		25.80						

(sh) = shoulder. <sup>a</sup> 0.1 M HCl. <sup>b</sup> MQ water. <sup>c</sup> 'Apparent' pK<sub>a</sub> value.**Fig. 3** Typical absorption and fluorescence emission spectra of compound **6** ( $\lambda_{\text{exc.}} = 397$  nm) in buffer at pH = 7 and pH = 1 (bottom).

The typical UV-Vis spectral response of **6** at different pH values, and the corresponding titration curves are shown in Fig. 4. The relationship between the absorbance and pH is sigmoidal, so data points were fitted to the Boltzmann function eqn (2):

$$A = A_2 + \frac{A_1 - A_2}{1 + \exp\left(\frac{\text{pH} - \text{pK}_{\text{a,app}}}{dx}\right)} \quad (2)$$

where  $A$  is the measured absorbance,  $A_2$  is the maximum absorbance,  $A_1$  is the minimum absorbance, and  $dx$  is the

width in pH units of the most significant change in absorbance. The curve exhibits excellent adjustment ( $R^2 = 0.9978$ ).

The acid-base properties are characterized by an 'apparent' pK<sub>a</sub> value (as opposed to a real thermodynamic pK<sub>a</sub>, since pH titrations were not performed under strictly controlled conditions of temperature and ionic strength), and are shown in Table 2. Unlike **3** and **5** which show pK<sub>a,app</sub> values of 2.91 and 2.7, respectively, both **4** and **6** show two values for pK<sub>a,app</sub> (2.7 and 7.9 for **4**, and 3.45 and 9.14 for **6**). This indicates that over the pH range examined, **4** and **6** exist in different pH sensitive forms which are spectrally detectable, from neutral molecules to dications, as demonstrated later by the computations.

### Titration with metal chloride salts

In order to evaluate the chemosensing ability of the studied amino and diamino substituted benzimidazo[1,2-*a*]quinolines **3–6** for the analytical detection of cations in aqueous solutions, their interaction with Co<sup>2+</sup>, Cu<sup>2+</sup>, Ni<sup>2+</sup> and Zn<sup>2+</sup> cations was evaluated through UV-Vis and fluorescence spectrophotometric titrations. Stock solutions of compounds were prepared in ethanol, while, during the titrations, small aliquots of stock solutions were added in MQ aqua at room temperature. Preliminary UV-Vis titrations were performed at the system concentration of  $2 \times 10^{-5}$  mol dm<sup>-3</sup> and  $1.5 \times 10^{-5}$  mol dm<sup>-3</sup>, while metal chloride salts were added in increasing concentrations, from  $1 \times 10^{-5}$  mol dm<sup>-3</sup>,  $2 \times 10^{-5}$  mol dm<sup>-3</sup>, and  $5 \times 10^{-5}$  mol dm<sup>-3</sup> up to  $1 \times 10^{-4}$  mol dm<sup>-3</sup>. Selected representatives are presented in Fig. 5.

System **3** showed a decrease in absorbance intensity proportional to the concentration of Zn<sup>2+</sup> (15% at both 422 and 449 nm) and Cu<sup>2+</sup> cations (21% at 448 nm and 15% at 421 nm). We also noticed a slight (around 5 nm) bathochromic shift of both absorption maxima upon the addition of Ni<sup>2+</sup>. Moreover, **5** revealed a decrease in the absorbance intensity upon increasing the concentration of Zn<sup>2+</sup> (21% at both 380 and 398 nm) and Ni<sup>2+</sup> cations (20% at both 378 nm and 398 nm). Systems **4** and **6**



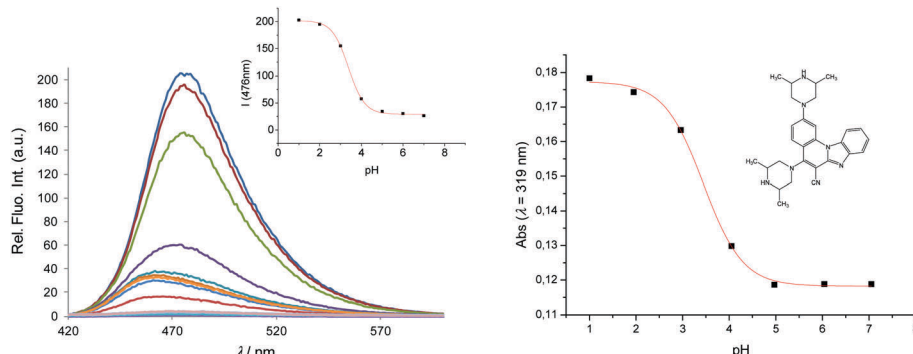


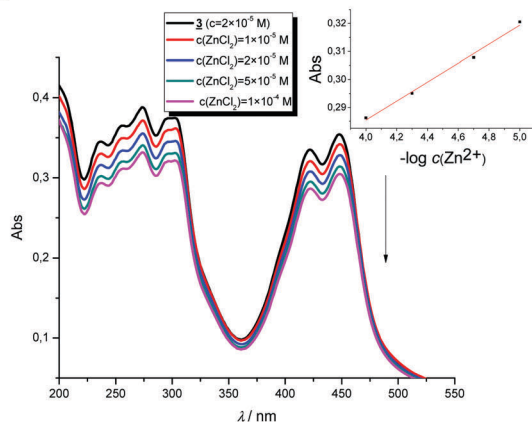
Fig. 4 Fluorescence emission spectra of **6**,  $2 \times 10^{-6}$  mol dm $^{-3}$  at different pH values (left) and its calibration curve (right); absorbance versus pH at 319 nm.

showed very small or negligible changes in the absorbance intensity upon the addition of the cation. Our preliminary comparative fluorimetric titrations with the same metals were performed at the concentrations of  $1 \times 10^{-7}$  mol dm $^{-3}$  for **3** and  $5 \times 10^{-7}$  mol dm $^{-3}$  for **4**, **5** and **6**. Some selected results are presented in Fig. 6, which suggest that **3–6** display a consistent decrease in the fluorescence intensity with the addition of metal cations at concentrations from  $1 \times 10^{-7}$  to  $1 \times 10^{-5}$  mol dm $^{-3}$ . Interestingly, Cu $^{2+}$  and Zn $^{2+}$  induced the largest intensity quenching

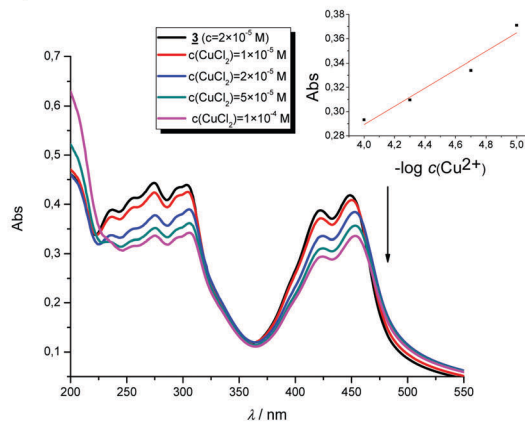
in **5**, being 65% and 59%, respectively, while in **6** the effect of these two metals is significantly surpassed by the other two metals, namely Co $^{2+}$  and Ni $^{2+}$ , assuming 34% and 39%, in the same order (Fig. 7), providing potential for different applications of these two systems.

In conclusion, we employed Job's continuous variation method<sup>33</sup> to reveal the metal binding stoichiometry of **3–6**. In doing so, we utilized the Cu $^{2+}$  cation, which is selected as a representative example, to provide support for the computational

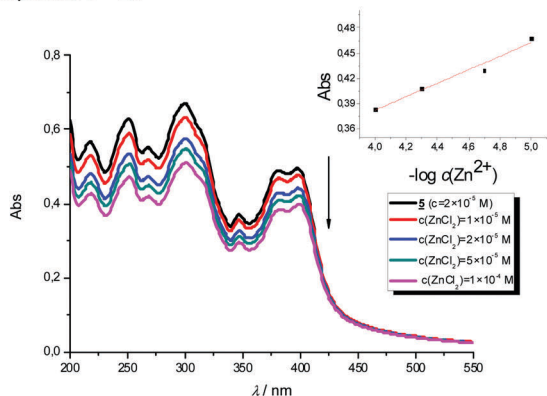
a) Compound **3** + Zn $^{2+}$



b) Compound **3** + Cu $^{2+}$



c) Compound **5** + Zn $^{2+}$



d) Compound **5** + Ni $^{2+}$

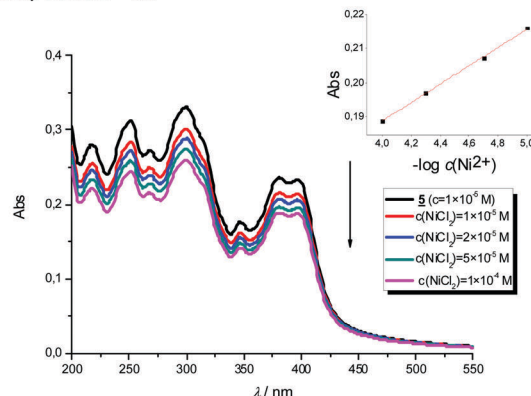


Fig. 5 UV-Vis titrations of compound **3** with Zn $^{2+}$  (a) and Cu $^{2+}$  cations (b) and titrations of compound **5** with Zn $^{2+}$  (c) and Ni $^{2+}$  cations (d). The insets show approximately linear decrease in absorption with the logarithm of the metal concentration.



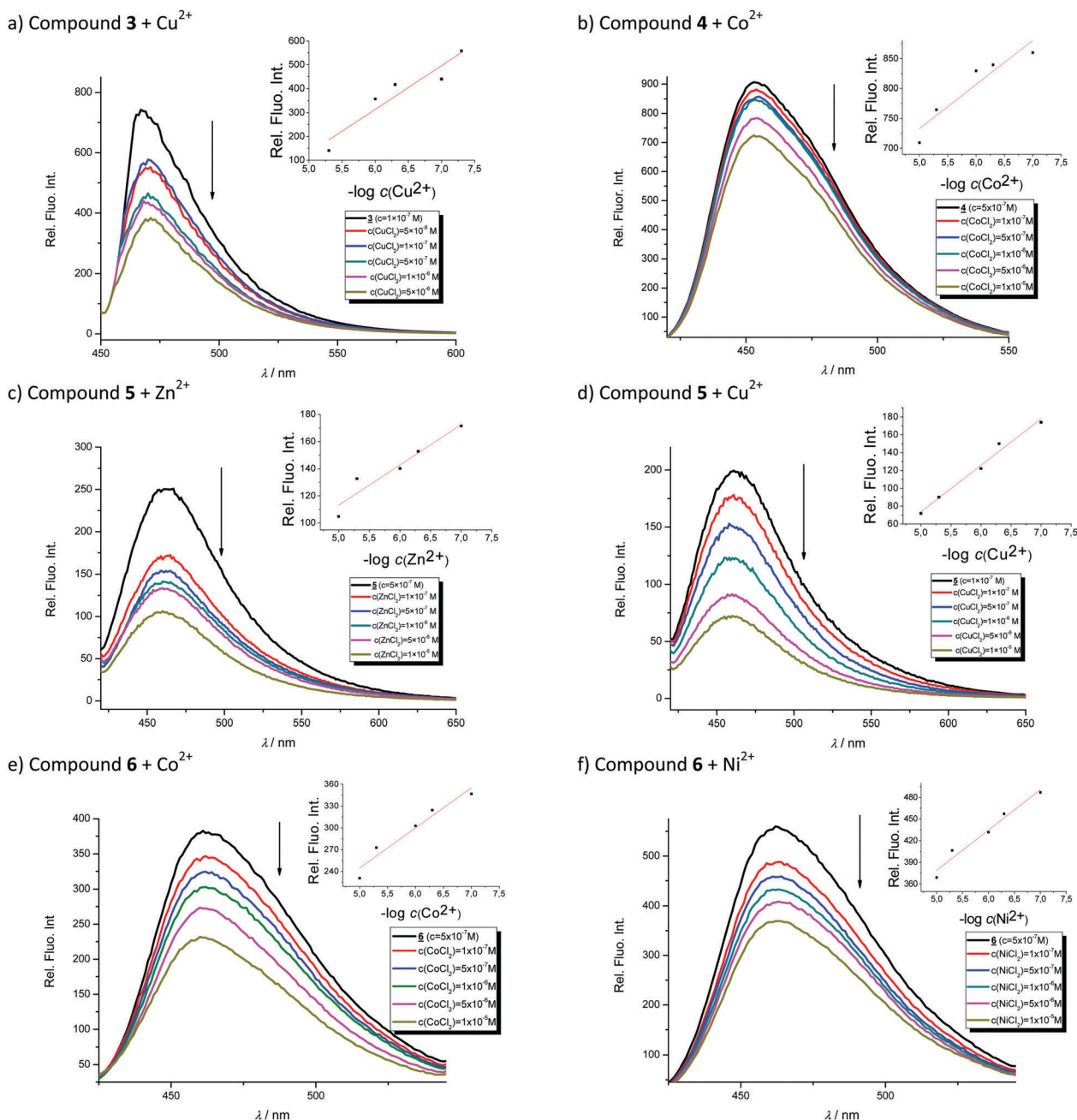


Fig. 6 Fluorimetric titrations of compound **3** with Zn<sup>2+</sup> (a), **4** with Co<sup>2+</sup> (b), **5** with Zn<sup>2+</sup> (c) and Cu<sup>2+</sup> (d) and **6** with Co<sup>2+</sup> (e) and Ni<sup>2+</sup> cations (f). The insets show approximately linear decrease in fluorescence intensity with the logarithm of the metal concentration.

analysis presented later. All four plots in Fig. S1 (ESI<sup>†</sup>) show a maximum intensity at the mole fraction of Cu<sup>2+</sup> of 0.5 strongly implying 1 : 1 complexation.

### Computational analysis

To rationalize the protonation states and the corresponding pK<sub>a</sub> values of the investigated systems, and to aid in interpreting how the latter are affected by metal cations, we performed a computational analysis using the B3LYP DFT functional and implicit SMD solvation corresponding to pure water. The calculated pK<sub>a</sub> values (Table 3) reveal that the

selected computational methodology is very successful in predicting these parameters. In comparison with the six measured values, the average absolute deviation is only 0.4 pK<sub>a</sub> units with the largest difference of 0.7 pK<sub>a</sub> units for the first protonation of **6**, which is remarkable. This lends credence to the rest of the computational data presented here.

Data in Table 3 suggest that the calculated acid/base properties could classify the investigated systems into two separate groups. Namely, **3** and **5** having chain amino substituents show differences in several distinct features from those of **4** and **6** bearing cyclic piperazine amino fragments. **3** and **5** are weakly acidic.



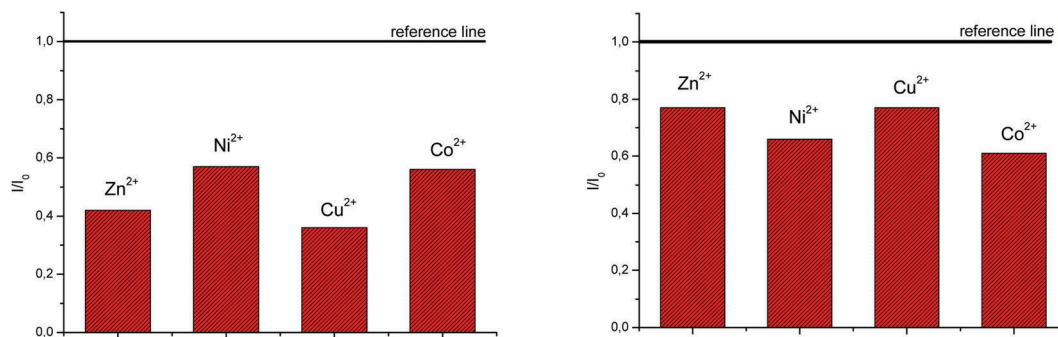
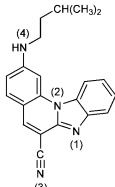
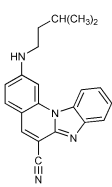
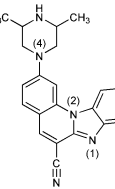
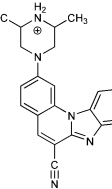
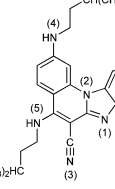
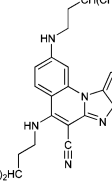
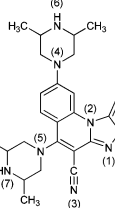
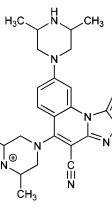


Fig. 7 The selectivity of chemosensors **5** (left) and **6** (right) and towards different cations.

Table 3 Calculated aqueous solution  $pK_a$  values for each protonation state of investigated systems. Shaded protonation states indicate the dominant form at the neutral pH = 7.0

System	Protonation state	$pK_a$ (calc) <sup>a</sup>	Protonation reaction	Structure at pH = 7
	$3^-$	23.7	$N4^- \rightarrow N4-H$	
	<b>3</b>	2.6 [2.91]	$N1 \rightarrow N1-H^+$	
	$3^+$	-6.0	$N4-H \rightarrow N4-H_2^{2+}$	
	$3^{2+}$	-22.3	$N3 \rightarrow N3-H^+$	
	$3^{3+}$	-38.1	$N1-H^+ \rightarrow N1-H_2^{2+}$	
	$3^{4+}$	-42.9	$N2 \rightarrow N2-H^+$	
	$3^{5+}$			
	$4^-$	39.2	$N6^- \rightarrow N6-H$	
	<b>4</b>	8.1 [7.89]	$N6-H \rightarrow N6-H_2^+$	
	$4^+$	2.1 [2.70]	$N1 \rightarrow N1-H^+$	
	$4^{2+}$	-6.5	$N4 \rightarrow N4-H^+$	
	$4^{3+}$	-23.1	$N3 \rightarrow N3-H^+$	
	$4^{4+}$	-39.8	$N1-H^+ \rightarrow N1-H_2^{2+}$	
	$4^{5+}$	-69.8	$N2 \rightarrow N2-H^+$	
	$5^{2-}$	28.7	$N4^- \rightarrow N4-H$	
	$5^-$	21.1	$N5^- \rightarrow N5-H$	
	<b>5</b>	3.2 [3.3]	$N1 \rightarrow N1-H^+$	
	$5^+$	-1.1	$N4-H \rightarrow N4-H_2^+$	
	$5^{2+}$	-13.4	$N5-H \rightarrow N5-H_2^+$	
	$5^{3+}$	-26.9	$N3 \rightarrow N3-H^+$	
	$5^{4+}$	Unstable		
	$6^{2-}$	40.4	$N6^- \rightarrow N6-H$	
	$6^-$	38.8	$N7^- \rightarrow N7-H$	
	<b>6</b>	9.8 [9.14]	$N7-H \rightarrow N7-H_2^+$	
	$6^+$	3.9 [3.45]	$N6-H \rightarrow N6-H_2^+$	
	$6^{2+}$	0.5	$N1 \rightarrow N1-H^+$	
	$6^{3+}$	-3.5	$N4 \rightarrow N4-H^+$	
	$6^{4+}$	-11.9	$N5 \rightarrow N5-H^+$	
	$6^{5+}$	-26.7	$N3 \rightarrow N3-H^+$	
	$6^{6+}$	-42.3	$N1-H^+ \rightarrow N1-H_2^{2+}$	
	$6^{7+}$	-71.3	$N2 \rightarrow N2-H^+$	
	$6^{8+}$			

<sup>a</sup> Experimental data measured in this work are given in square brackets.

Deprotonation of **3** to  $3^-$  is associated with  $pK_a = 23.7$ , while **5** is slightly more acidic ( $pK_a = 21.1$ ) because deprotonation occurs on the amino group next to the cyano moiety which is known to exhibit a strong acidifying effect.<sup>34</sup>

Still, deprotonation of **4** and **6** is much more difficult and it would require very strong bases with a  $pK_a$  of  $> 40$  in water. More importantly, the first protonation of **3** and **5** occurs on the imidazole imino nitrogen with the  $pK_a$  values of 2.6 and 3.2,

respectively, with **5** being slightly more basic due to the electron donating effect of the additional neighbouring amino group that promotes basicity.<sup>35</sup> The former is expected knowing that benzimidazole ( $pK_a = 5.49$ ) is more basic than, for example, *N*-methylaniline ( $pK_a = 4.85$ ) and *N*-ethylaniline ( $pK_a = 5.12$ ).<sup>36</sup> One also observes that the basicity of both **3** and **5** is lower than that of benzimidazole, which we attribute to the unfavourable effect of the attached cyano group. The second protonation



of **3** and **5** takes place on the substituent amino group further away from the cyano moiety; the  $pK_a$  values were calculated as  $-6.0$  and  $-1.1$ , respectively. This points to an important conclusion that, in water under normal conditions ( $pH = 7$ ), both **3** and **5** are predominantly present as unionized neutral molecules, which will turn out to be the major and significant difference compared to **4** and **6** (see later).

The first protonation of **4** and **6** occurs on the unsubstituted piperazine nitrogen corresponding to the  $pK_a$  values of  $8.1$  and  $9.8$ , respectively, with the latter molecule already being appreciably basic and even surpassing the basicity of the isolated piperazine ( $pK_a = 9.73$ ).<sup>36</sup> This leads to a conclusion that, unlike **3** and **5**, in aqueous solution systems **4** and **6** are predominantly monocations, which is an important observation. Interestingly, the second protonation of **4** occurs on the imino nitrogen ( $pK_a = 2.1$ ), while in **6** it takes place on the other piperazine unit ( $pK_a = 3.9$ ), which is only then followed by the imino protonation ( $pK_a = 0.5$ ) to yield  $6^{3+}$ .

The calculated differences in the acid/base features of **3** and **5** on one hand, and **4** and **6** on the other, help rationalize their different spectral properties, which is in excellent agreement with the observed spectral shifts induced by protonation with HCl (Table 2). Namely, introducing HCl into the solution of either **3** or **5** gives monoprotonated systems, which causes a hypsochromic (blue) shift of the absorption band. In contrast, for **4** and **6**, it produces diprotonated  $4^{2+}$  and  $6^{2+}$ , which increases the stability of systems through the enhanced electron redistribution and cationic resonance resulting in the bathochromic (red) shift. In this context, it is worth underlining the highest proton accepting abilities of **6**, for which the data in Table 3 indicate a relative ease in forming even tri- and tetra-protonated systems  $6^{3+}$  and  $6^{4+}$ , with the corresponding equivalents of even moderately strong acids. This would be evident in the absorption spectra, thus suggesting **6** as the most promising framework for the efficient pH sensor in the broad range of pH values.

In order to discuss the spectroscopic features of **3–6**, energies of the excited states responsible for the experimental UV/Vis spectra in Fig. 1 were calculated using the TD-DFT method (Fig. S4, ESI†). The results reveal that the TD-DFT method quite well reproduced a trend within a very narrow range of the absorption maxima, which are for **6**, taken as a representative example, calculated at  $389$ ,  $388$ ,  $386$  and  $387$  nm in toluene, dioxane, ethanol and acetonitrile, respectively (Fig. S4 and S8, ESI†), which is in reasonable agreement with the measured values of  $400$ ,  $399$ ,  $399$  and  $397$  (Table 1), in the same order. This is despite the fact that calculations show only a single band in the visible region in all solvents (Fig. S4, ESI†), while experiments display multiple bands in the same region (Fig. 1). In accounting this discrepancy, we note that the simulated spectra were obtained from pure vertical transitions without calculating vibronic contributions.<sup>37</sup> Although vibronic transitions certainly affect the band shapes, we assume that the inaccuracies are more likely related to the recently reported problems with the low lying  $\pi-\pi^*$  states of heteroaromatic molecules in TD-DFT calculations.<sup>38</sup> As explained by Prlj *et al.*,<sup>38</sup> the problem is in the unbalanced description of single and double excitations, which

can, depending on the problem, result in both under- and overestimated energy differences between the first two  $\pi-\pi^*$  transitions. Here, they are only overestimated with well-reproduced energies of the lowest transitions. We note in passing that variations in the DFT functional and basis sets had no significant impact on our results.

Nevertheless, the calculated  $\lambda_{\max}$  values show a reasonable correlation with the experimental values when all four systems **3–6** in all four organic solvents are considered (Fig. S8, ESI†). Differences between the lowest transition energies of **3–6** are in good correlation with the shifts of their lowest bands. Similarities between the experimental spectra of monosubstituted **3** and **4**, and between disubstituted **5** and **6**, are also present in the calculated spectra (Fig. S4, ESI†). On the other hand, the pronounced solvent effects of ethanol on **3** and of toluene on **6** were not found in the TD-DFT results. These effects must be due to some specific interactions with solvent molecules which are not involved at the present computational modeling level. It can be noted that similar solvents, like acetonitrile with **3**, and dioxane with **6**, did not produce a notable difference from other solvents. The spectral differences between mono- and diprotonated **6** (Fig. 3 and Fig. S5, ESI†) were also well reproduced in terms of the lowest transition energies, while agreement in relative intensities is modest.

We considered in more detail the excited states of **6**, which is a representative example among the two piperazine derivatives with markedly better analytical features. The nature of the calculated excitations of **6** and its protonation forms was checked using the recently proposed  $\phi_s$  descriptor.<sup>39</sup> For all states with the oscillator strength  $\geq 0.1$  (termed active states),  $\phi_s$  values were safely above  $0.4$  – the proposed threshold for states with significant charge transfer.<sup>39</sup> Only a few other states (with negligible intensities) were close to this value. Although TD-DFT energies somewhat deviate from the exact values, the difference densities are very likely less affected and well outlined here. The difference densities (obtained by subtracting the ground state from the excited state density) of all active states are dominated by  $\pi$ -electron contributions from the central benzimidazole–quinoline part extended by the peripheral nitrogen atoms and the cyano group (Fig. S6, ESI†). The densities are approximately symmetric across the conjugation plane, which almost looks as a nodal plane, thus indicating that  $\sigma$ -electrons hardly participate in the lowest electronic transitions. Difference densities for the most intense transitions are not influenced much by the solvent; in almost all cases, their relative order is also the same (Fig. S6, ESI†). Beside the conjugated part, photoinduced density redistribution in **6** involves, to a lesser extent, a transfer to piperazine rings. The second transition involves charge transfer from quinoline to the proximal part of the 5-piperazine, which is also active in few higher transitions, in contrast to mostly inactive 2-piperazine (apart from the linking nitrogen atom). Rydberg states were not present among the active sites. The nature of the four lowest active states is also well preserved in the neutral and two protonated species of **6** (Fig. S7, ESI†), despite chemical perturbation by protonation.



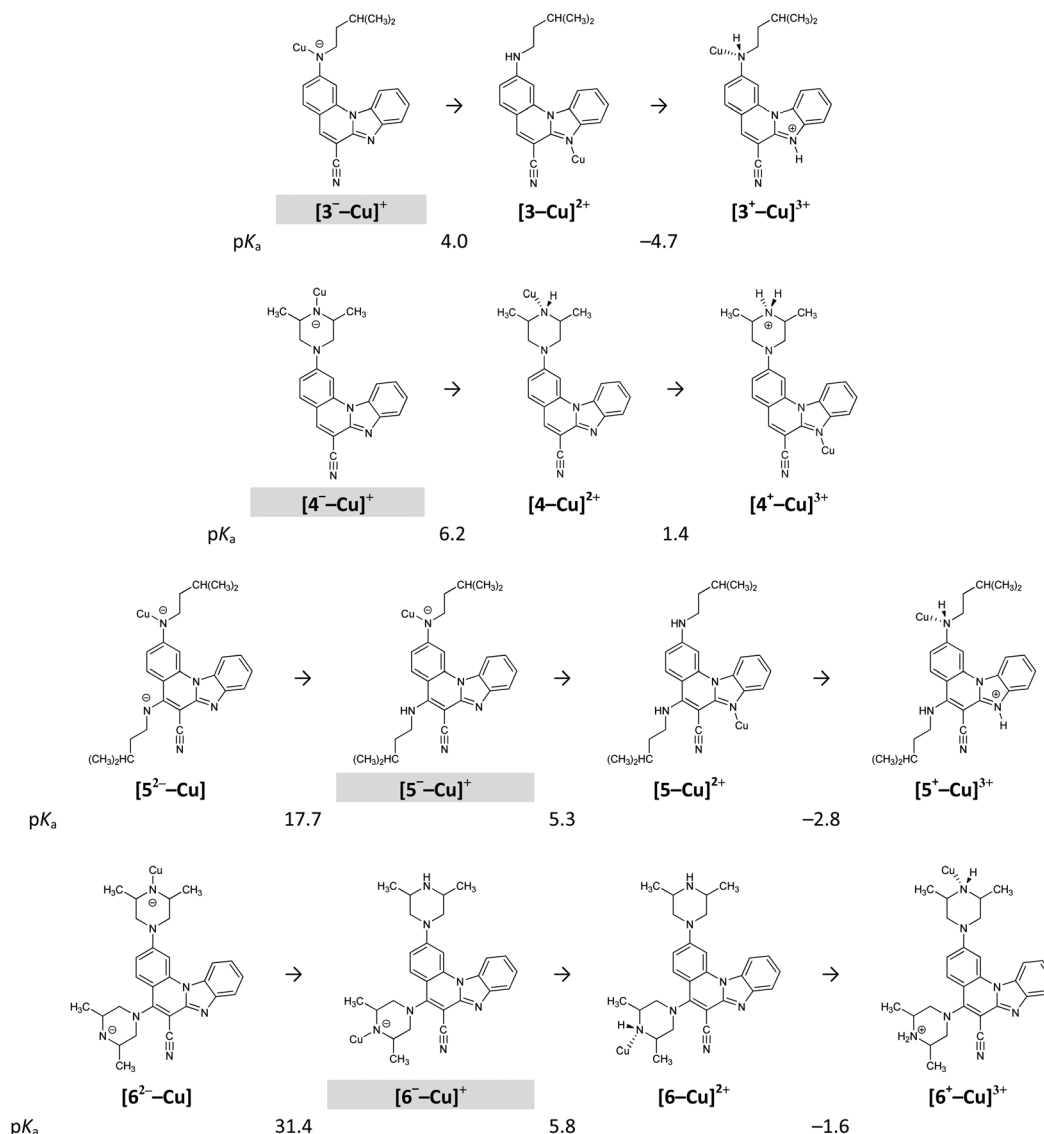


Fig. 8 Calculated  $pK_a$  values for the investigated systems in the presence of the  $Cu^{2+}$  ions. Shaded protonation states indicate the dominant form at neutral pH = 7.0.

The different acid/base properties of 3–6 are also reflected in their capabilities to bind metal cations, modelled here with the  $Cu^{2+}$  ions in a 1:1 ratio, in accordance with the experiments presented earlier. The presence of  $Cu^{2+}$  significantly alters the  $pK_a$  values of 3–6 (Fig. 8) as it favours their deprotonation so that, under normal conditions, all four systems are monoanions with  $Cu^{2+}$  bound to the most acidic site (Fig. 8). Since all 3–6 behave in the same way in this respect and assume the same monoanionic protonation state with  $CuCl_2$ , this explains why their UV-Vis spectra show considerable similarities and no clear spectroscopic distinction among molecules is obvious.

However, different behaviours are evident if one considers the strength of the interaction of the monoanionic 3<sup>−</sup>–6<sup>−</sup> with  $Cu^{2+}$ . It turns out that deprotonated piperazine nitrogen in 4<sup>−</sup> and 6<sup>−</sup> forms significantly stronger interaction with  $Cu^{2+}$  than nitrogen of the chain amine fragment in 3<sup>−</sup> and 5<sup>−</sup>. This is demonstrated in the calculated interaction free energies with

the  $Cu^{2+}$  ion, which in  $[M-Cu]^{+}$ , where  $M = 3-6$ , are  $-46.4$ ,  $-69.8$ ,  $-44.5$  and  $-70.5$  kcal mol<sup>−1</sup>, respectively. The second deprotonation of  $[5^{-}-Cu]^{+}$  and  $[6^{-}-Cu]^{+}$  is associated with the  $pK_a$  values of 17.7 and 31.4. This implies that it could occur under appreciably basic conditions, still much milder than without the  $Cu^{2+}$  ions, where it is associated with the  $pK_a$  values of 28.7 and 40.4, respectively (Table 3). This is a general trend, in which the  $Cu^{2+}$  ions increase the acidity of a particular amino centre by around 10 orders of magnitude, in accordance with our previous observations for the glutathione tripeptide and the  $Cd^{2+}$  ions.<sup>40</sup> Interestingly, only moderately strong acids are required ( $pK_a$  between 4–6) to revert the monoanionic 3<sup>−</sup>–6<sup>−</sup> to their unionized forms (Fig. 8), which is worth further studies towards utilizing these systems as potential pH sensors in the presence of the metal cations and *vice versa*, since somewhat stronger acids ( $pK_a$  between 2–4) are required to change the protonation state of 3–6 without the metal ions (Table 3).



## Conclusions

In this work novel 2-amino and 2,5-diamino substituted benzimidazo[1,2-*a*]quinolines 3–6 were synthesized in order to study their optical properties. UV-Vis and fluorescence spectroscopic characterizations were performed in polar and non-polar solvents as well as pH- and different metal chloride titrations in water.

The UV-Vis absorption spectra of 3–4 showed two main bands at 380–440 nm, while 5–6 displayed three main bands at 360–420 nm, which can be assigned to  $\pi$ - $\pi^*$  and  $n$ - $\pi^*$  electronic transitions, while bands at 250–325 nm correspond to the excitation of the conjugated  $\pi$ -system. 3 displayed the largest absorbance intensity in ethanol, while in other solvents significant hypsochromic effects were observed. 4 showed a hyperchromic effect in the absorbance intensity and a slight hypsochromic shift in non-polar solvents and ethanol, similarly to 5. 6 demonstrated the highest absorbance intensity in acetonitrile and a decreased intensity in toluene.

Emission spectra suggest that, in polar solvents, all systems exhibit fluorescence intensity quenching except 5, which showed the highest intensity in ethanol. In addition, the fluorescence quantum yield is strongly influenced by both the position and the type of the amino substituent on the tetracyclic framework. Thus, 2-*N*-isopentylamino substituted 3 revealed the highest quantum yield while 2,5-diamino derivatives showed very low yields (0.04 for 5 and 0.01 for 6).

The acid–base properties of 3–6 were examined and their pH sensing applicability was evaluated. All compounds exhibited spectral changes in the pH range 1–12 and a very strong pH sensitivity of fluorescence (in the range 450–500 nm), the latter making them promising candidates for efficient pH sensors. The bathochromic shift of the fluorescence emission band and a strong increase of the fluorescence intensity of 3, 4 and 6 occur on exposure to acidic solutions. It was found that 3–6 have potential for application in the acidic environment ( $pK_{app}$  in the range 2.70–3.45).

In order to determine the chemosensing ability of new systems, their interactions with  $Co^{2+}$ ,  $Cu^{2+}$ ,  $Ni^{2+}$  and  $Zn^{2+}$  cations were evaluated in 1:1 complexes. All compounds recognize metal cations in solution, as evidenced by the quenching of fluorescence intensity and a decrease in the UV-Vis absorbance, still without a significant practical selectivity among cations. The exception is offered by 5 and 6, in which a much higher relative intensity decrease was observed with  $Cu^{2+}$  and  $Zn^{2+}$ , and  $Co^{2+}$  and  $Ni^{2+}$  cations, respectively.

Computational analysis aided in rationalizing the acid/base features of the investigated molecules and their abilities to bind metal cations. The study of the  $pK_a$  values revealed that 3–6 could be divided into two distinct groups, which is experimentally evidenced in their different spectral properties, particularly in the shift of the absorption band in the visible spectrum. Namely, 3 and 5 having chain amino substituents are unionized under normal conditions, and upon the addition of HCl become monoprotonated at the corresponding imino centres to exhibit the hypsochromic (blue) shift of the absorption band. In contrast, 4 and 6 are significantly more basic and are predominantly

monocations, which become diprotonated in the same acidic media resulting in the bathochromic (red) shift.  $Cu^{2+}$  addition favours monodeprotonation in all 3–6 under normal conditions, which diminishes their differences in spectral responses, however, it produces systems which become more sensitive to very mild changes in the solution pH values (around  $pH \approx 4$ –6, as opposed to  $pH \approx 2$ –4 without the metal ions) opening the door for utilizing these systems as potential pH sensors in the presence of metal cations and *vice versa*.

## Experimental section

### Synthesis

**General methods.** All chemicals and solvents were purchased from commercial suppliers Acros, Aldrich or Fluka. Melting points were recorded on SMP11 Bibby and Büchi 535 apparatus. The  $^1H$  and  $^{13}C$  NMR spectra were recorded on a Varian Gemini 300 or Varian Gemini 600 at 300, 600, and 150 and 75 MHz, respectively. All NMR spectra were measured in  $DMSO-d_6$  solutions, while chemical shifts are reported in ppm ( $\delta$ ) relative to TMS as the internal standard. Mass spectra were recorded on an Agilent 1200 series LC/6410 QQQ instrument. The electronic absorption spectra were recorded on a Varian Cary 50 spectrometer using a quartz cuvette (1 cm). All systems were routinely checked by TLC using Merck silica gel 60F-254 glass plates. Microwave-assisted synthesis was performed in a Milestone start S microwave oven using quartz cuvettes under a pressure of 40 bar, and a power of 800 W at 170 °C. Elemental analyses for C, H and N were performed on a Perkin-Elmer 2400 analyzer. Where analyses are reported with element symbols, analytical results are within 0.4% of the theoretical values.

**General method for the preparation of systems.** Systems 3–6 were prepared according to previous reports,<sup>41</sup> using microwave irradiation at optimized power and reaction time, from the corresponding halogeno substituted systems in acetonitrile (10 mL) with the excess of the matching amine.

**2-*N*-i-Pentylaminobenzimidazo[1,2-*a*]quinoline-6-carbonitrile 3.** 3 was prepared from 1 (80 mg, 0.30 mmol) and isopentylamine (0.25 mL, 2.15 mmol) after 5 h of irradiation to yield 29 mg (29%) of yellow crystals; m.p. 200–205 °C.  $^1H$  NMR (300 MHz,  $DMSO-d_6$ ):  $\delta$  8.50 (d,  $J = 8.4$  Hz, 1H,  $H_{arom.}$ ), 8.46 (s, 1H,  $H_{arom.}$ ), 7.94 (dd,  $J_1 = 1.4$  Hz,  $J_2 = 7.8$  Hz, 1H,  $H_{arom.}$ ), 7.80 (d,  $J = 8.9$  Hz, 1H,  $H_{arom.}$ ), 7.74 (s, 1H,  $H_{arom.}$ ), 7.57 (dt,  $J_1 = 1.0$  Hz,  $J_2 = 7.4$  Hz, 1H,  $H_{arom.}$ ), 7.51 (dt,  $J_1 = 1.3$  Hz,  $J_2 = 7.5$  Hz, 1H,  $H_{arom.}$ ), 7.31 (t,  $J = 5.2$  Hz, 1H, NH), 6.90 (dd,  $J_1 = 1.7$  Hz,  $J_2 = 8.9$  Hz, 1H,  $H_{arom.}$ ), 3.32 (q,  $J = 7.1$  Hz, 2H,  $CH_2$ ), 1.80–1.75 (m, 1H, CH), 1.57 (q,  $J = 6.9$  Hz, 2H,  $CH_2$ ), 0.98 (d,  $J = 6.5$  Hz, 6H,  $CH_3$ ) ppm;  $^{13}C$  NMR (150 MHz,  $DMSO-d_6$ ):  $\delta$  153.8, 145.9, 144.2, 140.1, 138.1, 132.8, 130.4, 124.3, 122.3, 119.5, 116.7, 114.3, 111.2, 92.0, 40.6, 37.3, 25.2, 22.4 (2C) ppm; elemental analysis: found C 76.93, H 5.99, N 17.08%;  $C_{21}H_{20}N_4$  requires C 76.80, H 6.14, N 17.06%; MS (ESI):  $m/z = 329.3$  ( $[M + 1]^+$ ).

**2-[*N*-(3,5-Dimethylpiperazinyl)]benzimidazo[1,2-*a*]quinoline-6-carbonitrile 4.** Compound 4 was prepared from 1 (90 mg,



0.34 mmol) and 2,6-dimethylpiperazine (0.150 g, 1.30 mmol) after 6 h of irradiation to yield 39 mg (33%) of yellow powder; m.p. 263–268 °C. <sup>1</sup>H NMR (300 MHz, DMSO-*d*<sub>6</sub>): δ 8.47 (s, 1H, H<sub>arom.</sub>), 8.43 (dd, *J*<sub>1</sub> = 1.2 Hz, *J*<sub>2</sub> = 7.1 Hz, 1H, H<sub>arom.</sub>), 7.94 (dd, *J*<sub>1</sub> = 1.4 Hz, *J*<sub>2</sub> = 7.6 Hz, 1H, H<sub>arom.</sub>), 7.84 (d, *J* = 9.1 Hz, 1H, H<sub>arom.</sub>), 7.68 (s, 1H, H<sub>arom.</sub>), 7.58 (dt, *J*<sub>1</sub> = 1.2, *J*<sub>2</sub> = 6.6 Hz, 1H, H<sub>arom.</sub>), 7.53 (dt, *J*<sub>1</sub> = 1.3 Hz, *J*<sub>2</sub> = 6.7 Hz, 1H, H<sub>arom.</sub>), 7.27 (dd, *J*<sub>1</sub> = 1.7 Hz, *J*<sub>2</sub> = 9.1 Hz, 1H, H<sub>arom.</sub>), 4.01 (d, *J* = 10.5 Hz, 2H, CH<sub>2</sub>), 2.95–2.90 (m, 2H, CH), 2.55 (d, *J* = 11.7 Hz, 2H, CH<sub>2</sub>), 1.13 (d, *J* = 6.2 Hz, 6H, CH<sub>3</sub>) ppm; <sup>13</sup>C NMR (75 MHz, DMSO-*d*<sub>6</sub>): δ 154.2, 146.1, 144.5, 140.1, 138.5, 132.7, 130.7, 125.2, 123.3, 120.1, 116.9, 115.1, 112.9, 112.5, 97.8, 94.5, 53.6 (2C), 50.6 (2C), 19.5 (2C) ppm; elemental analysis: found C 74.40, H 6.08, N 19.52; C<sub>22</sub>H<sub>21</sub>N<sub>5</sub> requires C 74.34, H 5.96, N 19.70%; MS (ESI): *m/z* = 356.3 ([*M* + 1]<sup>+</sup>).

**2,5-Di-(*N*-*i*-pentylamino)benzimidazo[1,2-*a*]quinoline-6-carbonitrile 5.** Compound 5 was prepared from 2 (200 mg, 0.72 mmol) and *i*-pentylamine (0.17 mL, 1.50 mmol) after 6 h of irradiation to yield 34 mg (28%) of white powder; m.p. 111–113 °C. <sup>1</sup>H NMR (300 MHz, DMSO-*d*<sub>6</sub>): δ 8.27 (d, *J* = 8.2 Hz, 1H, H<sub>arom.</sub>), 8.13 (d, *J* = 9.3 Hz, 1H, H<sub>arom.</sub>), 7.68 (d, *J* = 7.5 Hz, 1H, H<sub>arom.</sub>), 7.62 (s, 1H, H<sub>arom.</sub>), 7.61 (t, *J* = 5.7 Hz, 1H, NH), 7.38 (t, *J* = 7.7 Hz, 1H, H<sub>arom.</sub>), 7.28 (t, *J* = 7.8 Hz, 1H, H<sub>arom.</sub>), 6.93 (t, *J* = 4.6 Hz, 1H, NH), 6.78 (d, *J* = 9.3 Hz, 1H, H<sub>arom.</sub>), 3.85 (q, *J* = 6.9 Hz, 2H, CH<sub>2</sub>), 3.26 (q, *J* = 7.5 Hz, 2H, CH<sub>2</sub>), 1.81–1.69 (m, 2H, CH), 1.66 (q, *J* = 7.1 Hz, 2H, CH<sub>2</sub>), 1.55 (q, *J* = 6.8 Hz, 2H, CH<sub>2</sub>), 0.97 (d, *J* = 5.3 Hz, 6H, CH<sub>3</sub>), 0.94 (d, *J* = 5.3 Hz, 6H, CH<sub>3</sub>) ppm; <sup>13</sup>C NMR (150 MHz, DMSO-*d*<sub>6</sub>): δ 157.7, 150.9, 150.1, 145.0, 136.9, 130.8, 130.5, 125.9, 123.5, 120.9, 118.3, 117.9, 113.1, 108.1, 104.8, 96.8, 40.6, 40.1, 38.4, 37.5, 25.3, 25.2, 22.4 (4C) ppm; elemental analysis: found C 75.37, H 7.54, N 17.09; C<sub>26</sub>H<sub>31</sub>N<sub>5</sub> requires C 75.51, H 7.56, N 16.93%; MS (ESI): *m/z* = 414.3 ([*M* + 1]<sup>+</sup>).

**2,5-Di-[*N*-(3,5-dimethylpiperazinyl)]benzimidazo[1,2-*a*]quinoline-6-carbonitrile 6.** Compound 6 was prepared from 2 (100 mg, 0.36 mmol) and 2,6-dimethylpiperazine (0.100 g, 0.90 mmol) after 3 h of irradiation to yield 51 mg (32%) of yellow powder; m.p. 233–236 °C. <sup>1</sup>H NMR (300 MHz, DMSO-*d*<sub>6</sub>): δ 8.27 (d, *J* = 7.9 Hz, 1H, H<sub>arom.</sub>), 7.86 (d, *J* = 9.4 Hz, 1H, H<sub>arom.</sub>), 7.81 (d, *J* = 7.6 Hz, 1H, H<sub>arom.</sub>), 7.61 (s, 1H, H<sub>arom.</sub>), 7.47 (t, *J* = 7.7 Hz, 1H, H<sub>arom.</sub>), 7.41 (t, *J* = 7.3 Hz, 1H, H<sub>arom.</sub>), 7.23 (dd, *J*<sub>1</sub> = 1.4 Hz, *J*<sub>2</sub> = 9.7 Hz, 1H, H<sub>arom.</sub>), 3.95 (d, *J* = 10.7 Hz, 2H, CH<sub>2</sub>), 3.54 (d, *J* = 11.0 Hz, 2H, CH<sub>2</sub>), 3.07 (m, 2H, CH), 3.00 (d, *J* = 11.3 Hz, 2H, CH<sub>2</sub>), 2.89 (m, 2H, CH), 2.46 (d, *J* = 9.5 Hz, 2H, CH<sub>2</sub>), 1.11 (d, *J* = 6.2 Hz, 6H, CH<sub>3</sub>), 1.05 (d, *J* = 6.18 Hz, 6H, CH<sub>3</sub>) ppm; <sup>13</sup>C NMR (75 MHz, DMSO-*d*<sub>6</sub>): δ 157.7, 153.6, 148.7, 145.0, 138.7, 130.6, 129.3, 124.7, 122.4, 119.3, 117.2, 114.4, 112.0, 109.6, 101.5, 98.1, 59.3 (2C), 53.6 (2C), 51.4 (2C), 50.5 (2C), 19.6 (2C), 19.2 (2C) ppm; elemental analysis: found C 71.72, H 7.15, N 21.13; C<sub>28</sub>H<sub>33</sub>N<sub>7</sub> requires C 71.92, H 7.11, N 20.97%; MS (ESI): *m/z* = 468.2 ([*M* + 1]<sup>+</sup>).

### Spectroscopic characterization

UV-Vis absorption spectra were recorded, against the solvent, at (25 ± 0.1) °C, using a Varian Cary 50 spectrophotometer in double-beam mode. The wavelength range covered was

200–500 nm. Quartz cells of 1 cm path length were used throughout and the absorbance values were recorded at 0.1 nm. Fluorescence measurements were carried out on a Varian Cary Eclipse fluorescence spectrophotometer at 25 °C using 1 cm path quartz cells. Excitation maxima were determined from excitation spectra covering the range of 200–500 nm. Emission spectra were recorded from 400 to 600 nm and corrected for the effects of time- and wavelength-dependent light-source fluctuations using a standard of rhodamine 101, a diffuser provided with the fluorimeter and the instrument software. The measurements were done in ethanol, acetonitrile, toluene and dioxane (HPLC grade). Relative fluorescence quantum yields  $\phi$  were determined according to Miller using eqn (3):

$$\phi_x = \phi_s \times A_s D_x n_x^2 / A_x D_s n_s^2 \quad (3)$$

where *A* is the absorbance at the excitation wavelength, *D* is the area under the corrected emission curve, and *n* is the solvent refractive index. Subscripts *s* and *x* refer to standard and unknown, the former being quinine sulphate with a fluorescence quantum yield of 0.54.<sup>28</sup> All samples were purged with argon to displace oxygen. The quantum yield reproducibility after three independent measurements was better than 10%.

### pH titrations

In order to study the effect of pH on the spectroscopic properties of 3–6, UV-Vis and fluorescence emission spectra were recorded in universal buffer solutions covering the pH range 2–12. Solutions of 0.1 M hydrochloric acid and 0.1 M sodium hydroxide were used as terminal acidic and basic points in the titration experiments with 1 × 10<sup>−5</sup> mol dm<sup>−3</sup> solutions of 3–6 for the absorbance and 2 × 10<sup>−6</sup> mol dm<sup>−3</sup> for the fluorescence measurements. The excitation wavelengths were determined from the absorption spectra.

### Computational details

As a good compromise between accuracy and feasibility, computational analysis was performed using the B3LYP DFT functional employing the 6-31+G(d) basis set for the carbon, nitrogen and hydrogen atoms and the Stuttgart–Dresden (SDD) effective core potentials<sup>42</sup> for the inner electrons of copper atoms and its associated double- $\zeta$  basis set for the outer ones. Thermal corrections were extracted from the corresponding un-scaled frequency calculations to obtain the free energies reported here. Gas-phase results were further refined with a single-point energy calculation employing a more flexible 6-311++G(2df,2pd) basis set. To account for the solvation effects, we included the SMD polarisable continuum model<sup>43</sup> with all parameters for pure water, giving rise to the B3LYP/6-311++G(2df,2pd)/SDD/(SMD)/B3LYP/6-31+G(d)/SDD model. The choice of this computational setup was prompted by its success in reproducing the kinetic and thermodynamic parameters of various organic reactions,<sup>44</sup> and predicting accurate *pK<sub>a</sub>* values for similar organic systems.<sup>35,45</sup> *pK<sub>a</sub>* values were calculated in an absolute fashion employing a gas-phase proton free energy of *G*°(H<sup>+</sup>) = 6.28 kcal mol<sup>−1</sup> and an experimentally determined value for the proton solvation free energy of





$\Delta G_{\text{SOLV}}(\text{H}^+) = -265.9 \text{ kcal mol}^{-1}$  in water,<sup>46</sup> to be consistent with the value used by Truhlar and co-workers<sup>43</sup> in parameterizing the SMD model. The latter value includes the free energy change associated with moving from a gas-phase pressure of 1 atm to a liquid-phase concentration of 1 M of  $-1.89 \text{ kcal mol}^{-1}$ .

Excited state calculations were performed with the TD-DFT approach using the 6-31+G(d) basis set together with the M06 functional, which produced the best results among the four other DFT functionals tested here, namely B3LYP, CAM-B3LYP, PBE0 and  $\omega$ B97X-D. 32 lowest singlet electronic excitations were determined employing the IEF-PCM implicit solvation model on geometries optimized at the (SMD)/B3LYP/6-31+G(d) level. Descriptors for difference densities<sup>39</sup> were calculated using the program Nancy\_EX 2.0,<sup>47</sup> while all other calculations were performed using the Gaussian 09 software.<sup>48</sup>

## Acknowledgements

Financial support by the Croatian Science Foundation (project IP-2014-09-3386 entitled Design and synthesis of novel nitrogen-containing heterocyclic fluorophores and fluorescent nanomaterials for pH and metal-ion sensing) is gratefully acknowledged. D. B. and R. V. wish to thank the Zagreb University Computing Centre (SRCE) for granting computational resources on the ISABELLA cluster and the CRO-NGI infrastructure.

## Notes and references

- B. Wang and E. V. Anslyn, *Chemosensors: Principles, Strategies and Applications*, Wiley-VCH, Weinheim, 2011.
- B. Valeur, *Molecular fluorescence-principles and applications*, Wiley-VCH, Weinheim, 2002.
- U. S. Spichiger-Keller, *Chemical sensors and biosensors for medical and biological applications*, Wiley-VCH, Weinheim, 1998.
- P. A. Gale and C. Caltagirone, Anion Sensors, in *Chemosensors: Principles, Strategies and Applications*, ed. B. Wang and E. V. Anslyn, Wiley-VCH, Weinheim, 2011, pp. 395–427.
- Y. Jeong and J. Yoon, *Inorg. Chim. Acta*, 2012, **381**, 2–14.
- (a) E. V. Anslyn, *J. Org. Chem.*, 2007, **72**, 687–699; (b) B. T. Nguyen and E. V. Anslyn, *Coord. Chem. Rev.*, 2006, **250**, 3118–3127.
- (a) T. Gunnlaugsson, M. Glynn, G. M. Tocci, P. E. Kruger and F. M. Pfeffer, *Coord. Chem. Rev.*, 2006, **250**, 3094–3117; (b) C. Caltagirone and P. A. Gale, *Chem. Soc. Rev.*, 2009, **38**, 520–563.
- Y. Yang, Q. Zhao, W. Feng and F. Li, *Chem. Rev.*, 2013, **113**, 192–270.
- (a) D. W. Choi and J. Y. Koh, *Annu. Rev. Neurosci.*, 1998, **21**, 347–375; (b) Z. Xu, J. Yoon and D. R. Spring, *Chem. Soc. Rev.*, 2010, **39**, 1996–2006.
- (a) A. Ajayaghosh, P. Carol and S. Sreejith, *J. Am. Chem. Soc.*, 2005, **127**, 14962–14963; (b) A. E. Lee, M. R. Grace, A. G. Meyer and K. L. Tuck, *Tetrahedron Lett.*, 2010, **51**, 1161–1165.
- R. A. Lovstad, *BioMetals*, 2004, **17**, 111–113.
- D. Wencel, T. Abel and C. McDonagh, *Anal. Chem.*, 2014, **86**, 15–29.
- J. Han and K. Burgess, *Chem. Rev.*, 2009, **110**, 2709–2728.
- R. Wang, C. Yu, F. Yu and L. Chen, *TrAC, Trends Anal. Chem.*, 2010, **29**, 1004–1013.
- M. I. Stich, L. H. Fischer and O. S. Wolfbeis, *Chem. Soc. Rev.*, 2010, **39**, 3102–3114.
- W. Shi, X. Li and H. Ma, *Methods Appl. Fluoresc.*, 2014, **2**, 042001.
- M. Schaferling, *Angew. Chem., Int. Ed.*, 2012, **51**, 3532–3554.
- B. Valeur and I. Leray, *Coord. Chem. Rev.*, 2000, **205**, 3–40.
- A. P. de Silva, H. Q. N. Gunaratne, T. Gunnlaugsson, A. J. M. Huxley, C. P. McCoy, J. T. Rademacher and T. E. Rice, *Chem. Rev.*, 1997, **97**, 1515–1566.
- N. Dash, A. Malakar, M. Kumar, B. B. Mandal and G. Krishnamoorthy, *Sens. Actuators, B*, 2014, **202**, 1154–1163.
- Y. Q. Ge, J. Jia, H. Yang, X. T. Tao and J. W. Wang, *Dyes Pigm.*, 2011, **88**, 344–349.
- R. M. F. Batista, R. C. M. Ferreira, M. M. M. Raposo and S. P. G. Costa, *Tetrahedron*, 2012, **68**, 7322–7330.
- M. Hranjec, G. Pavlović, M. Marjanović, M. Kralj and G. Karminski-Zamola, *Eur. J. Med. Chem.*, 2010, **45**, 2405–2417.
- D. Y. Kim and H. J. Kim, *Sens. Actuators, B*, 2015, **206**, 508–515.
- A. Kumar, M. Chhatwal and T. Gupta, *Tetrahedron Lett.*, 2012, **53**, 5691–5694.
- S. H. Mashraqui, S. Sundaram and T. Khan, *Chem. Lett.*, 2006, **35**, 786–787.
- A. Mishra, S. Chatterjee and G. Krishnamoorthy, *J. Photochem. Photobiol., A*, 2013, **260**, 50–58.
- (a) M. Yu, H. Lin, G. Zhao and H. Lin, *J. Mol. Recognit.*, 2007, **20**, 69–73; (b) F. A. S. Chipem, S. K. Behera and G. Krishnamoorthy, *Sens. Actuators, B*, 2014, **191**, 727–733.
- N. Perin, M. Hranjec, G. Pavlović and G. Karminski-Zamola, *Dyes Pigm.*, 2011, **91**, 79–88.
- M. Hranjec, E. Horak, M. Tireli, G. Pavlović and G. Karminski-Zamola, *Dyes Pigm.*, 2012, **95**, 644–656.
- A. P. Demchenko, *Anal. Bioanal. Chem.*, 2009, **395**, 1195–1196.
- A. P. de Silva, H. Q. Nimal Gunaratne, T. Gunnlaugsson, A. J. M. Huxley, C. P. McCoy, J. T. Rademacher and T. E. Rice, *Chem. Rev.*, 1997, **97**, 1515–1566.
- (a) P. Job, *Ann. Chim.*, 1928, **9**, 113–203; (b) J. S. Renny, L. L. Tomasevich, E. H. Tallmadge and D. B. Collum, *Angew. Chem., Int. Ed.*, 2013, **52**, 11998–12013.
- (a) R. Vianello and Z. B. Maksić, *J. Org. Chem.*, 2010, **75**, 7670–7681; (b) R. Vianello and Z. B. Maksić, *New J. Chem.*, 2009, **33**, 739–748; (c) R. Vianello and Z. B. Maksić, *New J. Chem.*, 2008, **32**, 413–427.
- I. Despotović and R. Vianello, *Chem. Commun.*, 2014, **50**, 10941–10944.
- D. D. Perrin, B. Dempsey and E. P. Serjeant, *pKa Prediction for Organic Acids and Bases*, Chapman and Hall, London, 1981.
- F. Santoro and D. Jacquemin, *Wiley Interdiscip. Rev.: Comput. Mol. Sci.*, 2016, **6**, 460–486.
- A. Prlj, M. E. Sandoval-Salinas, D. Casanova, D. Jacquemin and C. Corminboeuf, *J. Chem. Theory Comput.*, 2016, **12**, 2652–2660.



- 39 (a) T. Etienne, X. Assfeld and A. Monari, *J. Chem. Theory Comput.*, 2014, **10**, 3896–3905; (b) T. Etienne, X. Assfeld and A. Monari, *J. Chem. Theory Comput.*, 2014, **10**, 3906–3914; (c) T. Etienne, *J. Chem. Theory Comput.*, 2015, **11**, 1692–1699.
- 40 M. Glušić, J. Stare, J. Grdadolnik and R. Vianello, *J. Inorg. Biochem.*, 2013, **119**, 90–94.
- 41 N. Perin, R. Nhili, K. Ester, W. Laine, G. Karminski-Zamola, M. Kralj, M. H. David-Cordonnier and M. Hranjec, *Eur. J. Med. Chem.*, 2014, **80**, 218–227.
- 42 D. Andrae, U. Häussermann, M. Dolg, H. Stoll and H. Preuss, *Theor. Chim. Acta*, 1990, **77**, 123–141.
- 43 A. V. Marenich, C. J. Cramer and D. G. Truhlar, *J. Phys. Chem. B*, 2009, **113**, 6378–6396.
- 44 (a) D. Saftić, R. Vianello and B. Žinić, *Eur. J. Org. Chem.*, 2015, 7695–7704; (b) I. Picek, R. Vianello, P. Šket, J. Plavec and B. Foretić, *J. Org. Chem.*, 2015, **80**, 2165–2173.
- 45 (a) M. P. Coles, P. J. Aragón-Sáez, S. H. Oakley, P. B. Hitchcock, M. G. Davidson, Z. B. Maksić, R. Vianello, I. Leito, I. Kaljurand and D. C. Apperley, *J. Am. Chem. Soc.*, 2009, **131**, 16858–16868; (b) R. J. Schwamm, R. Vianello, A. Maršavelski, M. Á. García, R. M. Claramunt, I. Alkorta, J. Saame, I. Leito, C. M. Fitchett, A. J. Edwards and M. P. Coles, *J. Org. Chem.*, 2016, **81**, 7612–7625.
- 46 M. D. Tissandier, K. A. Cowen, W. Y. Feng, E. Gundlach, M. H. Cohen, A. D. Earhart, J. V. Coe and T. R. Tuttle, *J. Phys. Chem. A*, 1998, **102**, 7787–7794.
- 47 Nancy\_EX-2.0 is a free post-processing tool for the analysis of the density and character of electronic excited states; <https://sourceforge.net/projects/nancyex/>, accessed Oct 15, 2016.
- 48 M. J. Frisch, G. W. Trucks, H. B. Schlegel, G. E. Scuseria, M. A. Robb, J. R. Cheeseman, G. Scalmani, V. Barone, B. Mennucci, G. A. Petersson, H. Nakatsuji, M. Caricato, X. Li, H. P. Hratchian, A. F. Izmaylov, J. Bloino, G. Zheng, J. L. Sonnenberg, M. Hada, M. Ehara, K. Toyota, R. Fukuda, J. Hasegawa, M. Ishida, T. Nakajima, Y. Honda, O. Kitao, H. Nakai, T. Vreven, J. A. Montgomery, Jr., J. E. Peralta, F. Ogliaro, M. Bearpark, J. J. Heyd, E. Brothers, K. N. Kudin, V. N. Staroverov, R. Kobayashi, J. Normand, K. Raghavachari, A. Rendell, J. C. Burant, S. S. Iyengar, J. Tomasi, M. Cossi, N. Rega, J. M. Millam, M. Klene, J. E. Knox, J. B. Cross, V. Bakken, C. Adamo, J. Jaramillo, R. Gomperts, R. E. Stratmann, O. Yazyev, A. J. Austin, R. Cammi, C. Pomelli, J. W. Ochterski, R. L. Martin, K. Morokuma, V. G. Zakrzewski, G. A. Voth, P. Salvador, J. J. Dannenberg, S. Dapprich, A. D. Daniels, Ö. Farkas, J. B. Foresman, J. V. Ortiz, J. Cioslowski and D. J. Fox, *Gaussian 09, Revision A.02*, Gaussian, Inc., Wallingford, CT, 2009.

